Journal of Engineering and Applied Sciences 13 (Special Issue 8): 6451-6461, 2018
ISSN: 1816-949X

Aerodynamic Characteristics of an Aerofoil in Wide Range of Angles of Attack

[1]Pavel V. Bulat, [2]Samuel Mitchell and [2]Konstantin N. Volkov
[1]Research Laboratory of "Shock Wave and Explosive Processes",
Federal State Budget Educational Institution of Higher Education,
"Baltic State Technical University, "Voenmeh" D.F. Ustinov",
Stepana Razina Street 7/78, St. Petersburg, Russia
[2]Department of Mechanical and Automotive Engineering, Kingston University, London, UK

Abstract: Calculation of the aerodynamic forces on the single aerofoil at different Angles of Attack (AOAs) is fundamental task in various engineering applications of fluid dynamics. Computational Fluid Dynamics (CFD) offers a way to model the complex flow features that occur during the operation. CFD simulation is used to determine the aerodynamic characteristics of a single aerofoil in a wide range of conditions.

Key words: Aerofoil, lift, drag, computational fluid dynamics, turbulence, stall

INTRODUCTION

The implementation of an innovative aerodynamic control technique is a point of extensive investigation, since, the conventional technology is reaching its limits. The main effort of the industry in the field of aerodynamics is related to the development of blades which offer better performance increased reliability and faster control.

Computational Fluid Dynamics (CFD) is used to model the performance of aerofoils through the solving of Navier-Stokes equations. While computationally intensive, CFD offers a way to model the complex flow features that occur during the operation of a turbine. The CFD simulations of aerofoils at high Angles of Attack (AOA) have been relatively rarely reported in the literature as they are not common in the application of general aerodynamic vehicles.

Direct Numerical Simulation (DNS) of turbulent flow is limited to low and moderate Reynolds numbers and simple geometry, due to the high computational cost of resolving all turbulent scales in the flow. The simulation based on Reynolds Averaged Navier-Stokes equations (RANS) where time averages (or statistical averages) are computed to an affordable cost with the drawback of introducing turbulence models based on parameters that have to be tuned for particular applications. An alternative to DNS and RANS is Large Eddy Simulation (LES) where only the largest scales of the flow are resolved, combined with Sub-Grid Scale (SGS) Models to take into consideration the effect of the smallest unresolved turbulent scales. SGS Models are explicit, based on physics theory or experiments or implicit through the numerical discretization of the equations (Sagaut, 2006).

The aerofoils operate in a wide range of AOAs (from 0-360°) including both unstalled and stalled conditions. At the high Reynolds numbers, boundary layers are turbulent and for small AOAs the flow is attached until the separation at the rear of the blade with small drag and high lift. Under increasing AOAs the flow stays attached with a corresponding increase in lift and drag, until stall is reached where the flow separation moves upstream which results in a decrease in lift and a dramatic increase in drag.

Using the Langley low-turbulence pressure tunnel, Critzos *et al.* (1955). Conducted tests on the NACA0012 aerofoil at AOAs from 0-180°. The aerofoil used in the investigation had a chord length of 0.1524 m and spanned the entire 0.914 m of the wind tunnel. Expressions from Abbott *et al.* were used to correct the results for the effects of the solid blockage. At a Reynolds number of $Re = 1.8\times10^6$ they found the maximum coefficient of lift to occur at an AOA of 14° and have a value of 1.33. A less abrupt peak in the coefficient of lift was seen to occur at an AOA approximately 45°. Similar peaks in the coefficient of lift were observed at 170 and 145° having magnitudes of 0.77 and 1.07, respectively. At 0° of AOA the coefficient of drag was observed to be 0.007 while at 180° it was 0.014. At 90° a value of 2.08 was recorded for the coefficient of drag which is similar to that obtained for a flat plate of infinite aspect

Corresponding Author: Pavel V. Bulat, Research Laboratory of "Shock Wave and Explosive Processes", Federal State Budget Educational Institution of Higher Education, " Baltic State Technical University, "Voenmeh" D.F. Ustinov", Stepana Razina Street 7/78, St. Petersburg, Russia

ratio. At a lower Reynolds number of Re = 5×10^5, the maximum coefficient of lift occurred earlier at an AOA of 10° and with a lower value of about 1. Between 20 and 125° the coefficient of lift was largely unaffected by the decrease in Reynolds number but beyond 125° the magnitude was seen to be lower. Overall this reduction in Reynolds number saw a decrease in the coefficient of drag, except for a range of AOA from 10 and 20° where the coefficient of drag increased from the value measured at a Reynolds number of Re = 1.8×10^6.

Probably, the most well-documented and widely adopted data for high incidence wind turbine applications is that by Sheldahl and Klimas (1981). They conducted experimental tests on the NACA0009, NACA0012, NACA0015 and NACA0012H aerofoils over a range of AOAs from 0-18° using a wind tunnel. They used aerofoils with a chord length of 0.1524 m for tests conducted at Reynolds numbers of Re = 3.6×10^5, 5×10^5 and 7×10^5 and an NACA0012 aerofoil with a chord length of 0.381 m for tests conducted at a Reynolds number of Re = 8.6×10^5, 1.36×10^6 and $1{:}76\times10^6$. They observed significant hysteresis features in the coefficient of lift measurements of the NACA0012 aerofoil at AOAs from 8-18°. These features were also, seen for the NACA0015 and NACA0012H aerofoils but not for the NACA0009 aerofoil. A comparison of the coefficient of tangential force curve for each aerofoil, calculated from their measurements of the coefficients of lift and drag, suggest the NACA0015 and NACA0012H aerofoils offer better performance when compared with the other aerofoils used in the experiment. For all aerofoils, it was found that beyond an AOA of 25°, neither Reynolds number nor geometry had much effect on the coefficient of lift. Similarly, for the coefficient of drag, beyond an AOA of 20° Reynolds number and geometry have little effect.

In addition Sheldahl and Klimas (1981) used their experimental findings to produce predictions of the aerodynamic characteristics of the NACA0018, NACA0021 and NACA0025 aerofoils for a range of Reynolds numbers from 10^4-10^7. Some hysteresis phenomenon is observed at the onset of the aerofoil stall depending on the initial condition if it is a fully stalled configuration (higher AOAs) or a fully attached condition (lower AOAs). Comprehensive experimental studies on the NACA0012 aerofoil were performed by Gregory and O'Reilly (1973) and Harris (1981). However, their works did not cover Reynolds numbers below Re = 1.44×10^6.

Four appropriate aerofoils were chosen for testing by Worasinchai *et al.* (2011). They conducted both experimental tests and CFD simulations on four different aerofoils: the symmetric NACA0012 and the asymmetric SG6043, SD7062 and DU06-W-200. Measurements of the aerodynamic characteristics of these aerofoils were taken at Reynolds numbers of Re = 6.5×10^4, 9×10^4 and 1.5×105. When comparing their experimental observations with CFD predictions for the NACA0012 aerofoil, they saw good agreement up to an AOA of 10°. Between 10 and 14°, however, CFD did not predict a surface separation bubble which was observed experimentally. They noted no significant difference in this phenomenon over the different Reynolds numbers. When comparing their observations with the work of Sheldahl *et al.* (1980), they noted some difference between their findings. Immediately after stall occurred, Sheldahl and Klimas (1980) observed the coefficient of lift dropped to almost zero. However, Worasinchai *et al.* (2011) observed a much smaller drop in the coefficient of lift to 0.6. They did not observe the peak in the coefficient of lift at an AOA of 45° to the same extent as Sheldahl *et al.* (1980) who saw this peak exceed the first pre-stall peak. In addition while Worasinchai *et al.* (2011) observed a discontinuity in the coefficient of lift at 54°, Sheldahl *et al.* (1980) did not. It might be an effect of the test studies configuration used in the experiments (closed or open test studies) as discussed by Worasinchai *et al.* (2011).

There was one significant difference in the coefficient of drag and that was the discontinuity observed by Worasinchai *et al.* (2011) at around 55° which was not observed by Sheldahl and Klimas (1980). Following this discontinuity, up until the corresponding AOA past 90 of 125°, the magnitude of the coefficient of drag was seen to be around 40% lower than observed by Sheldahl *et al.* (1980). Conclusions related to the asymmetric aerofoils that were tested suggested that the benefits of using cambered aerofoils (which have a delayed onset of stall) are partly negated by a reduction in performance which occurs when the aerofoil operates at an AOA between 180 and 360°.

The choice of turbulence models influences the computational results and the required computation resources. The RANS Models are wildly used in turbulence modelling with fair accuracy and efficiency. Among the various RANS Models, the Shear Stress (SST) model is the one combining the k-ϵ and k-ω Models based on the zonal blending functions. The SST Model is considered a promising approach for simulating flow with great adverse pressure gradients and separation. Compared with RANS, LES is more computationally demanding in which larger and boundary-dependent eddies are resolved directly through the governing equations and the influences of smaller and more

homogenous eddies are taken into account by a SGS Model. However, LES is compatible with a wider range of turbulent flows than RANS model as it retains the unsteady large-scale coherent structures.

At a high AOAs flow separation is known to occur so, a suitable turbulence model must be chosen. Eleni *et al.* (2012) found that the SST Model produces the best results of all steady state models following an evaluation of different turbulence models. Using particle imaging velocimetry, Ferreira *et al.* (2009) experimentally measured the development of flow over the leading edge of the NACA0015 aerofoil. They recorded vorticity shed from the leading edge of the aerofoil. Ferreira *et al.* (2010) used results of their experiments to validate further CFD simulations. The simulations compared different turbulence models (Spalart-Allmaras, k-ε) in RANS and LES and DES approaches. They found the Spalart-Allmaras Model underestimated the generation and shedding of vorticity at the leading edge and the k-ε Model did not predict the shed vortices accurately. The LES approach allowed to reproduce the vortex shedding but the area covered by these predicted vortices was larger than what was observed experimentally. The DES Model gave results which best agreed with the experimental data.

The flow around aerofoil at high AOA is unsteady and 3D separated with a nonlinear lift variation. Cummings *et al.* (2003) pointed out several important issues for the accurate simulation of high AOA flow fields such as turbulence modelling and domain dimensionality. For example, the URANS Models often fail to provide accurate results for high AOA flows where there is large-scale turbulence in separated flows. On the other hand, DES or LES, although, recognized as more advanced and powerful turbulence models are rarely found in the past CFD studies. The certain potential limitation in 2D CFD simulation is prone to be overlooked. For example, the flow diversities in spanwise direction of blades cannot be considered in 2D CFD simulations. Sorensen and Michelsen (2004) found that 2D Navier-Stokes solvers overpredict the lift and drag of the stalled aerofoil, even when AOA was only slightly above the stall angle. Quasi or full 3D simulation should be adopted to overcome the shortcoming of the conventional 2D Model. In quasi 3D CFD simulation approach, the 2D Model is extended in a spanwise direction for a considerable length in order to achieve a realistic reproduction of 3D separated vortices. The spanwise length is not fully modelled in such a 3D simulation, so that, it is referred to as 2.5D CFD simulation hereinafter in order to differentiate it from the conventional 2D and 3D simulations. Gao *et al.* (2008) performed 2.5D LES simulations of the flow field around a single static aerofoil and found that the 2D Model is not adequate for predicting unsteady flow structures with large-scale separations around aerofoils at relatively high AOAs. Im and Zha (2011) presented simulations of a single aerofoil beyond stall using the DES approach which is essentially a hybrid model of RANS and LES. Results of the 2.5 DES Model are clearly superior over those of the 2.5D URANS Models.

Mary and Sagaut (2002) conducted an LES with different spanwise extents and different numerical resolutions to simulate a flow past an aerofoil at Reynolds number of 2.1×10^6 and AOA of 13.3°. They found that there was a great improvement in the results compared with the experimental data when the width of the computational domain and the numerical resolution were increased. LES gives improvements of separation predictions and Li *et al.* (2013) found it to give best agreement with experimental results in comparison with the URANS Model when using it to simulate high AOA flow.

CFD simulations on a static NACA0018 aerofoil at a Reynolds number of $Re = 3\times10^5$ over a range of AOAs from 0-180° were performed by Li *et al.* (2013). They investigated the feasibility and accuracy of three different CFD approaches (2D URANS, 2.5D URANS and 2.5D LES) with a focus on the capability of the 2.5D LES approach in CFD simulation of high AOA flow. The 2.5D Model differs from a full 3D Model in that only a certain length of blades is modelled with periodic boundaries at the two extremities of the domain. URANS calculations were based on SST turbulence model and LES calculations were based on Smagorinsky-Lilly SGS Model. The aerofoil used had a chord length of 0.2 m. They used a circular domain with a radius of 30 chord lengths, a structured O-mesh and placed 280 cells along the aerofoil and 120 cells across the domain. A fine mesh was used, y plus values of less than one were ensured and the growth rate was limited to 1.08. Among the three methods, 2.5D LES yielded the best agreement with the experimental data reported by Claessens (2006). Detailed examinations of simulated flow field revealed that 2.5D LES produces more realistic 3D vortex diffusion after flow separation, resulting in more accurate predictions of aerodynamic coefficients in static or dynamic stall situations.

The coefficients of lift and drag predicted by Li *et al.* (2013) with 2.5 LES were close to those observed experimentally by Claessens (2006) for all AOAs except 15° which was due to the dynamic characteristic of the experiment. Li *et al.* (2013) found, however that the 2D and 2.5D URANS simulations significantly overpredicted the

lift in the stall region and also, the drag from 45-135°. In general, 2.5D LES showed good agreement with experimental results.

Several RANS and LES runs in near-stall and stall conditions were carried out by Moreau *et al.* (2008). The stall condition is found to have an extraneous sound source at low frequencies. It is characterized by two specific tones whose frequencies could correspond to the shear-layer instability followed by a von Karman vortex shedding, observed by Hoarau *et al.* (2006) in their DNS study at low Reynolds number. In general, the static stall angles of symmetric aerofoils range from 10-15° (Sheldahl and Klimas, 1981).

The results of RANS and LES numerical simulations of aerodynamic characteristics of a single NACA0012 aerofoil in a wide range of AOAs, from 0-180° are reported in this study. RAND calculations are performed using 2D domain and LES calculations are carried out in 3D domain with periodical boundary conditions in spanwise direction. RANS simulation is based on SST turbulence model and Smagorinsky-Lilly Model is applied to LES simulations. The results obtained are compared with experimental and numerical data from previous researches.

MATERIALS AND METHODS

Numerical simulations are performed to determine the aerodynamic characteristics of the aerofoil. Dimensionless force coefficients provide a convenient way to compare the aerodynamic characteristics of different aerofoils, regardless of their size and are given by $C_D = 2F_D/(\rho U^2 A)$ and $C_D = 2F_L/(\rho U^2 A)$ where F_L and F_D are lift and drag forces, U is the apparent flow velocity as seen by the aerofoil, ρ is the air density. The apparent flow velocity is a result of the aerofoil having motion relative to the flow. An aerofoil varies by way of length in the span-wise direction (Span, S) and length in the flow-wise direction (Chord, C). The reference area of the aerofoil is then given by A = CS.

The incompressible Navier-Stokes equations are appropriate because the resultant flow velocity has generally the mach number <0.3. Stall, either static or dynamic, may occur and both are dominatedby vortex separation and involve flow unsteadiness. Therefore, an unsteady fluid solver isnecessary to investigate such kinds of flow.

Figure 1 shows the geometric scheme and boundary conditions in the CFD Model of a single NACA0012 aerofoil. In 3D calculations, the domain is extruded some thickness in the spanwise direction depending on AOA. The inlet boundary is a semi-circular boundary with radius

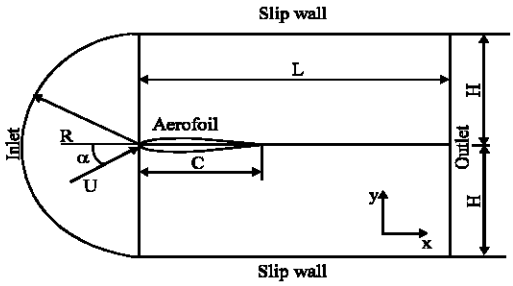

Fig. 1: Geometry of the computational domain and boundary conditions

R = 15C and centre located at the tip of the aerofoil when the AOA is 0°. The inlet boundary is located far away from the aerofoil to avoid wave reflection. The AOA is adjusted by rotating the aerofoil about the mid-point of the chord line and is measured relative to the x axis. The length of the domain is the distance from the aerofoil tip to the outlet and L = 30C.

Free stream velocity corresponding to the Reynolds number and degree of turbulence (about 5%) are specified on the inlet boundary. Top and bottom boundaries are treated as free-slip walls. No-slip and no-penetration boundary conditions are applied to the aerofoil. Non-reflecting boundary conditions are used on the outlet boundary. Periodic boundary conditions are used in spanwise direction. Due to the symmetrical nature of aerofoils and also to reduce computational expense, RANS investigation is performed in 2D domain. However, 3D domain is used for LES calculations with periodical boundary conditions in spanwise direction. Adequate mesh resolution is important to obtain an accurate solution and to ensure that the large eddies in the flow are resolved. Near-wall units (dimensionless distance from the wall relating to the first mesh point) are used to check the mesh resolution for a particular mesh.

SST turbulence model puts certain requirements on the properties of the mesh to enable the acquisition of an accurate flow prediction. In the near-wall region, the SST Model requires ayplus value of $y^+<2$. Another requirement of the SST Model is that the boundary layer must be resolved by at least 15 mesh points (or mesh layers). The first layer thickness that should yield a desired yplus and the boundary layer thickness are estimated using the semi-empirical correlations for the flat plate. The mesh resolution is optimized for the highest Reynolds number used in this study ($Re = 3.6\times10^5$).

LES usually needs streamwise and spanwise mesh resolutions based on wall units $x^+<50$ and $z^+<20$, respectively. The mesh is designed to give $y^+<1$ and to locate about 5 points in region where $y^+<5$.

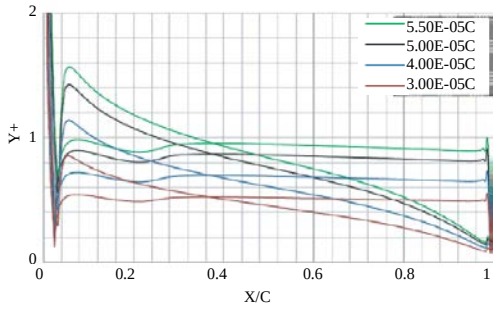

Fig. 2: Non-dimensional near-wall values along the aerofoil for various first layer thicknesses ($\alpha = 10°$, $Re = 3.6\times10^5$)

The RANS and LES simulations have been performed using a first layer thickness as low as 5×10^{-5}C. In all cases a growth rate of 1.2 is used for the inflation layer and it is ensured there are enough layers that the inflation layer entirely covers the boundary layer. In thecase of the chosen first layer thickness of 1.5×10^{-5}C, 26 layers were required to ensure the inflation layer completely covered the boundary layer. In all calculations, y-plus coordinate is uniformly distributed along aerofoil except small area near the stagnation point where yplus is about 1 in RANS and yplus is about 0.25 in LES. Distributions of yplus coordinate along aerofoil are presented in the Fig. 2.

Both O and C-mesh topologies can minimize the skewness of a near-wall mesh, avoid high aspect ratios of cells in the far wake and converge fast under a high-order discretization scheme.

A hybrid mesh is used in this study. The mesh contains a structured layer emanating from the surface of the aerofoil that contains sufficient points to model the flow as it interacts with the no-slip wall of the aerofoil and a tetrahedral unstructured mesh filling the rest of the domain. Sizing controls used include inflation emanating from the aerofoil surface, edge sizing along the aerofoil surface in the flow-wise direction, edge sizing in the span-wise direction, global growth rate, maximum face size, body of influence radius and body of influence sizing.

A mesh convergence study to find the optimum mesh parameters has been carried out on the standard NACA0012 aerofoil at an AOA of 10° and a Reynolds number of $Re = 3.6\times10^5$. These optimum parameters are given in Table 1.

In order to resolve the laminar sub-layer directly, the first mesh spacing on the aerofoil was determined to make yplus values <1. Mesh-stretching was limited to <1.12 in both streamwise and crossflow directions to ensure numerical stability.

Table 1: Mesh parameters

Variables	Values
Inflation layer	
First layer thickness	50×10^{-5}C
Number of layers	26
Growth rate	1.2
Aerofoil edge sizing	
Flow-wise	1.25×10^{-3}C
Span-wise	1
Body of influence	
Radius 1	4C
Sizing 1	5×10^{-2}C
Growth rate	1.12
Radius 2	2C
Sizing 2	2×10^{-2}C
Growth rate	1.12
Global parameters	
Max face size	0.6C
Growth rate	1.12
Statistics	
Number of nodes	175000
Number of cells	380000

The 3D Model differs from the 2D Model in the sense that it extends the model in a spanwise direction for a certain length. A pair of translational periodic conditions was enforced in spanwise direction. The 3D mesh consisted of 280 cells along the aerofoil wall, 120 cells in the normal direction to the wall and 40 cells uniformly distributed in the spanwise direction. The number of cells was determined through a mesh refinement study.

In the 3D Model, the aerofoil was extruded in a spanwise direction in order to reproduce 3D turbulence structures. Too small spanwise width makes the flow become virtually 2D rather than 3D. At low AOAs, a relatively short spanwise width (S = 0.074C) is sufficientto obtain results comparable with wind tunnel data whereas in high AOAs flow, a muchlonger width is needed to capture the larger 3D turbulence vortex separation and shedding structures. The spanwise width of 2C was selected in the 3D simulations and the mesh contains 20 layers in spanwise direction as recommended by Li *et al.* (2013). Since, periodic boundaries were enforced at the two ends of the domain in the spanwise direction, the actual spanwise variation in averaged physical quantities is almost negligible. A layer of inflation has been used to create a structured layer emanating from the aerofoil surface.

The segregated approach was selected to solve the discretized continuity and momentum equations and a second-order implicit formula was used for the temporal discretization. The SIMPLEC scheme was used to solve the pressure-velocity coupling. In the SST Model, the second-order upwind discretization scheme and third-order MUSCL discretization scheme were applied for pressure and other variables, respectively. In the LES model, the bounded central difference scheme was used for spatial discretization of the momentum. As a result, the

solutions were second-order accurate in the space and time domains. The steady state solution of the SST flow field was used as the initial condition of LES to accelerate the convergence.

Time step size is a crucial parameter in unsteady flow simulations. To get accurate results of an aerofoil beyond stall, Sorensen and Michelsen (2004) suggested the non-dimensional time steps $\tau = \Delta tU/C$ to be 0.01 (corresponding to the real time step $\Delta t = 0.0001$ s) to keep CFL<0.5. This time step was applied in the simulations of the single aerofoil. The flow was found to be statistically steady after 1 sec and aerofoil surface pressure was acquired in the following 2 sec which was equal to 222 flow-through times according to the free stream velocity and aerofoil chord length.

RESULTS AND DISCUSSION

The benchmark NACA0012 aerofoil is a symmetrical aerofoil with thickness-to-chord ratio of 12%. It was chosen for testing because it is one of few aerofoils for which wind tunnel data for the entire range of AOAs is available from Sheldahl and Klimas (1981).

Effect of AOA: The results obtained are validated against that which has been produced in previous experimental works and CFD predictions (Critzos *et al*., 1955; Sheldahl and Klimas, 1981; Kirke and Lazauskas, 2008; Dominy *et al*., 2007). Validation of the CFD results is performed at three different Reynolds numbers (3.6×10^5, 1.5×10^5 and 6.5×10^4) and in a wide range of AOAs from 0-180°.

The predictions of the aerodynamic characteristics of the NACA0012 made by CFD are compared to those measured in previous works. In addition to RANS, LES calculations were also performed and compared with RANS predictions in order to better understand the capability of LES.

Simulations have been performed for a range of AOAs from 0-180° in steps no >10° at $Re = 1.5\times10^5$ and $Re = 3.6\times10^5$. Figure 3 and 4 shows that overall there is a good similarity between the experimental measurements by Critzos *et al*. (1955), Sheldahl and Klimas (1981), Kirke and Lazauskas (2008) and the CFD predictions. At $\alpha = 30°$ there is excellent agreement between all observations and the CFD predictions but then at $\alpha = 40r°$ the CFD predicts sharp peaks in lift and drag which were not observed experimentally. The wind tunnel results show a hysteresis loop caused by a deep stall which may have been induced by the slow rolling of the aerofoil study in the wind tunnel experiments. In CFD simulations, the aerofoils at different AOAs were completely static and thus no such a hysteresis loop could be observed.

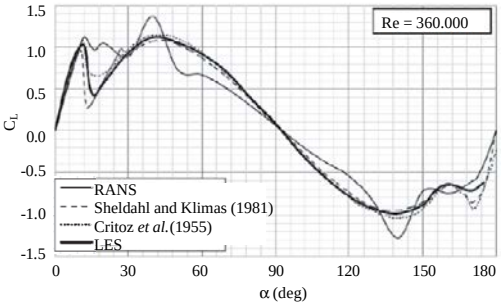

Fig. 3: Lift as a function of AOA at $Re = 3.6\times10^5$

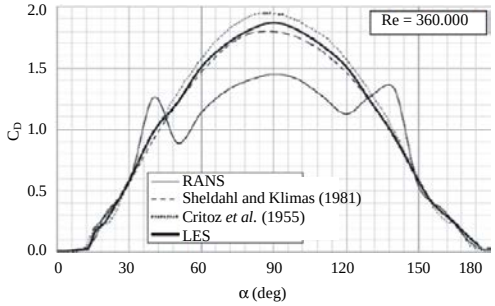

Fig. 4: Drag as a function of AOA at $Re = 3.6\times10^5$

On closer inspection, Fig. 5 shows excellent agreement with the experimental data in the prediction of lift from $\alpha = 0°$ up until stall occurs at $\alpha = 12°$. In the range $12°<\alpha<20°$ there is variation in all the data that has been compared but the CFD Model consistently predicts a higher value of lift than all the previous observations. Figure 5 also shows a good agreement for drag. However, the sharp rise that is observed experimentally between $12°<\alpha<16°$ is not predicted by the CFD Model.

However, similar peaks were observed by Dominy *et al*. (2007) at $Re = 1.5\times10^5$ as shown in Fig. 6 and 7. Beyond $\alpha = 40°$ up until $\alpha = 130°$ the CFD Model then underpredicts both lift and drag.

For $Re = 1.5\times10^5$ in the stall region CFD seems to overpredict lift compared to both Sheldahl and Klimas (1981) experimental findings and Dominy *et al*. (2007) CFD predictions. A peak in lift and drag similar to that predicted by Dominy *et al*. (2007) is observed but the peaks predicted by CFD are both larger and seem to occur earlier. Again, CFD underpredicts d rag compared to Sheldahl and Klimas (1981) for the remainder of AOAs.

A relatively good agreement is seen between the sets of data in the pre-stall regime. Theygive almost identical lift coefficient peak values, although, the Sheldahl and Klimas (1981) data show a slightly earlier stall. After the stall, the lift from the RANS calculations fallsto a value of

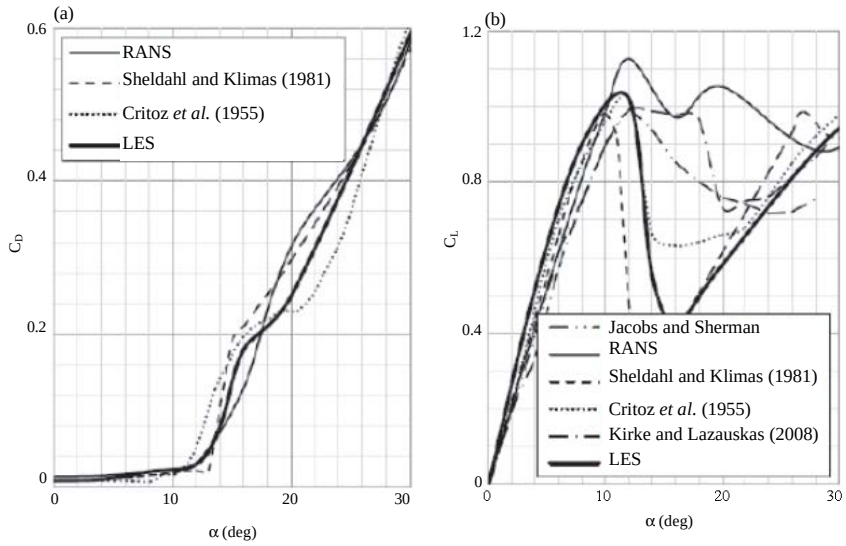

Fig. 5: a) Lift and b) Drag as a function of AOA at Re = 3.6×10^5

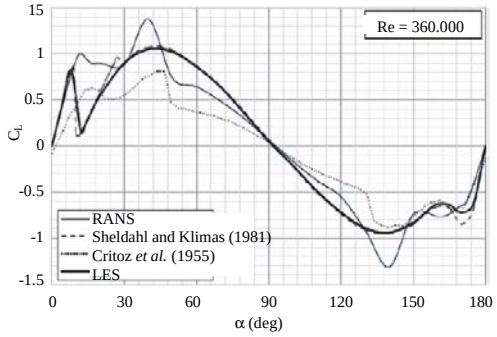

Fig. 6: Lift as a function of AOA at Re = 1.5×10^5

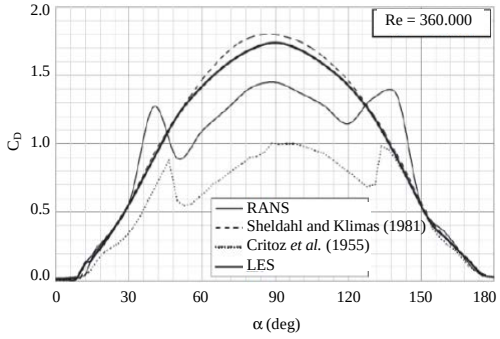

Fig. 7: Drag as a function of AOA at Re = 1.5×10^5

around 0.7, maintaining and gradually increasing that value with increasing AOA to 56°. The experimental lift curve shows a quite different post-stall characteristicin which the lift drops to almost zero before sharply rising to the second peak. It is notclear what physical flow mechanism could result in such a dramatic lift loss and recovery in the immediate post-stall zone and it is unfortunate that this feature was not discussed by Sheldahl and Klimas (1981) in their original work.

Figure 3 and 4 shows the results of the mean lift and drag coefficients for thestudied NACA0012 aerofoil obtained with RANS and LES as well as the wind tunnel testresults. Both the computational and experimental Reynolds numbers were equal to 3.6×10^5.The stall starts at 12° and ends at 16°. In this process, the separation is initiated at thetrailing edge of the aerofoil and shifts forward to the leading edge with increasing AOA whereas the lift force is kept almost constant.

At low (pre-stall) AOAs, both RANS computations using the SST turbulence model and LES agree with the experimental results well. However, at high (post-stall) AOAs, RANS results underpredict drag and lift substantially deviates from the experimental results at 40 and 130°. RANS Model provides accurate results for attached boundary layer flowsbut fails to simulate the large-scale turbulence in separated flows. Therefore, the RANS Model is not suitable for resolving flow if the AOA is >15°. Compared with the RANS Model, the LES shows anexcellent agreement with the wind tunnel results from 0-140°.

Effect of Reynolds number: The effect that the Reynolds number has on the aerodynamic characteristics of the NACA0012 aerofoil is investigated. Three different Reynolds numbers are used (Re = 3.6×10^5, Re = 1.5×10^5 and Re = 6.5×10^4). The inlet velocity is adjusted to produce each Reynolds number simulation. Figure 8 and 9 show that at most AOAs, the lift and drag is not dependentupon the Reynolds number.

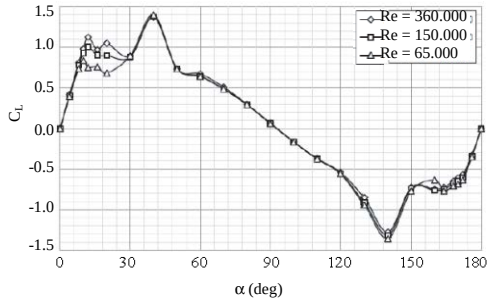

Fig. 8: Lift as a function of AOA at varying Reynolds numbers

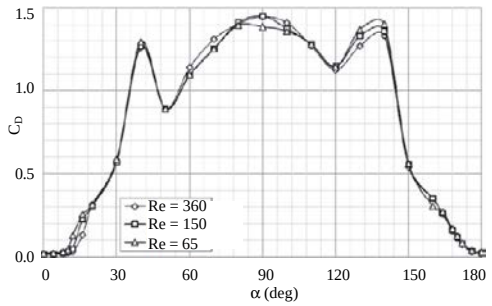

Fig. 9: Drag as a function of AOA at varying Reynolds numbers

However, there are certain AOAs where the values of lift and drag are Reynolds number dependent. Specifically, these are in the range of AOA from 8-30° and can be seen in greater detail in Fig. 10. As the Reynolds numberis reduced, so, too is the lift. In addition as the Reynolds number is reduced the dragincreases. Stall occurs earlier as the Reynolds number is reduced. All these findings arein agreement with previous studies reported by Critzos *et al.* (1955), Gregory and O'Reilly (1973), Sheldahl *et al.* (1980) and Worasinchai *et al.* (2011).

The mean static pressure on the surface, characterized by the pressure coefficient provides a more quantitative assessment of the accuracy of the various simulations. To observe how the flow varies for these AOAs that show a dependency upon the Reynolds number it is useful to analyse pressure variations both on the aerofoil surface (Fig. 11-13). The two RANS simulations at 10 and 12° clearly shows an attached flow with very close loading. At 216°, the flat pressure distribution on the suction side is a sign of the aerofoil stall. The pressure levels are however, slightly higher than the experimental one. Looking at what happens for an AOA of 10°, at Re = 3.6×10^5 results shows there is no flow separation occurring. At the lower Reynolds number of Re = 1.5×10^5 separation has just started to occur on the upper surface of the trailing edge but is barely visible

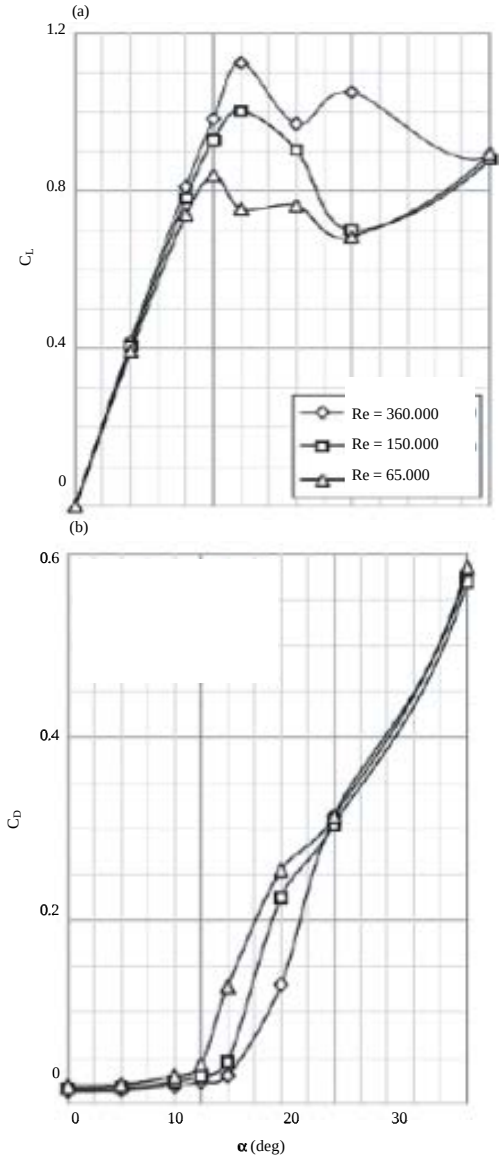

Fig. 10: a) Lift and b) Drag as a function of AOA at varying Reynolds numbers

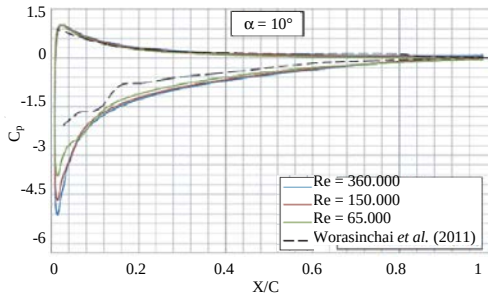

Fig. 11: Pressure coefficient along aerofoil as a function of distance from leading edge for α = 10°

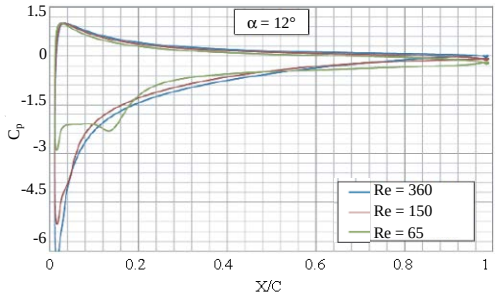

Fig. 12: Pressure coefficient along aerofoil as a function of distance from leading edge for α =12°

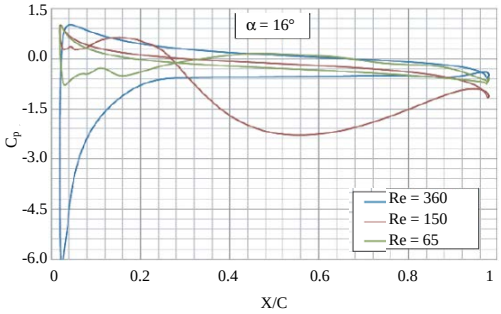

Fig. 13: Pressure coefficient along aerofoil as a function of distance from leading edge for α = 16°

on the streamline graphic. At Re = 6.5×10^4 the trailing edge separation is slightly larger. In addition, the streamline pattern shows separation has just started to occur on the uppersurface of the leading edge which can also be identified by the discontinuity of the coefficientof pressure plot along the aerofoil surface in Fig. 11-13.

For an AOA of α = 12° the streamline pattern shows separation on the upper surface ofthe trailing edge has just started to occur at Re = 3.6×10^5 while at Re = 1.5×10^5 separationat the upper trailing edge has become more visible. The plot of pressure coefficient along the aerofoil surface shows that separation at the leading edge has just started to occur too. At Re = 6.5×10^4 the trailing edge separation has extended all the way along the uppersurface to meet the leading edge separation.

For an AOA of α = 16° the streamline plot at Re = 3.6×10^5 now resembles that of α = 12° at Re = 1.5×10^5 with the trailing edge separation extending along the uppersurface. However, there is still no sign of any leading edge separation. At Re = 1.5×10^5 and Re = 6.5×10^4, transient features have started to occur and it would seem as thoughthe vortices are being shed from the upper surface of the aerofoil. The monitor plots of liftand drag show clear periodic oscillations.

The results obtained show that the lift curves in pre-stall are not significantly affected by the Reynolds

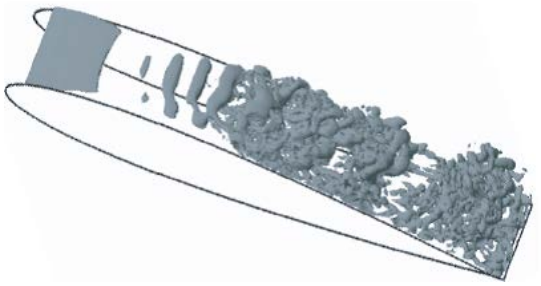

Fig. 14: Isosurfaces of Q criterion at Q = 200

number. The maximum lift coefficients occur at 12° AOA for all Reynolds numbers but the peak lift coefficient is seen to increase with Reynolds number to maximaof 0.802, 0.925 and 1.210 for the three tested Reynolds numbers. This maximum lift iscomparable to the value of 0.853 measured by Sheldahl and Klimas (1980) at the Reynolds number of 1.6×10^5.

With further small AOA increase, the flow separates over the entire aerofoil surface and the lift drops rapidly to a value of approximately 0.64 before gradually increasing again to 1.45 at around 45°. There is a further drop in lift at 54°, followed by further gradual reduction to zero at 90°. The fall in lift corresponds to a sudden change of flow behaviour, particularly on the suction side. In this stalled flow, the suction side pressure remains almost constant over the entire surface but there is a significant change in the magnitude of that pressure coefficient between 50 and 60°.

These trends are reversed as the AOA passes 90° and the aerofoil is travelling backwards. In terms of drag, the usual pre-stall trend is followed as the AOA increases. Drag coefficients decrease slightly with increasing Reynolds number. Drag then increases sharplyat the stall point, corresponding to the observed reduction in lift and continues to increaserapidly to a peak at approximately 48°. Further AOA increase results in a rapid fall in drag. Although, the peak drag magnitude appears to be Reynolds number sensitive, all three testsshow a fall to about the same value of drag. The drag then increases again reaching a secondpeak at 90°. Above 90°, the trend is reversed.

In order to illustrate the three-dimensionality of the flow, the vortex structures were identified and visualized using the Q-method (Joeng and Hussain, 1995). The Q criterion isthe second invariant of the velocity gradient tensor. Positive values of the Q criterion locate regions in which rotation dominates over strain rate. Figure 14 shows the 3D isosurfaces of the Q criterion over the upper surface of the aerofoil from LES solution. The process of breakdown to turbulence is

captured in the LES and the results obtained are in qualitative agreement with the DNS results reported by Jones *et al.* (2008) for low Reynolds numbers. Starting from the leading edge, the shear layeris detached from the aerofoil surface with laminar 2D behaviour. Transition to turbulencebecomes visible as a small distortion of the shear layer and the 3D of the flow starts to grow. Large-scale structures form and then break down into small structures followed by fully 3D turbulent flow. There are spanwise variations of the flow structures and these structurescould not be captured by the LES in narrow domain.

CONCLUSION

RANS and LES of flow over an aerofoil were performed in a wide range of AOAs. Validation with experimental data for the aerodynamic characteristics of the single NACA0012 aerofoilhas shown reasonable agreement, although, some notable differences were observed. A single static aerofoil was simulated using the LES and the results were compared with those obtained from wind tunnel experiments as well as RANS simulations. The comparisons demonstrated that the RANS Model considerably overpredicted the lift and drag of the single aerofoil at post-stall AOAs due to the inaccurate vorticity diffusion behaviour described bythe 2D Navier-Stokes equations. In contrast to RANS, LES provided a much better agreement with the experimental results and a more realistic description of the aerodynamic details. The RANS simulations remained almost 2D in such highly separated flows whereas the 3D LES could capture theessential pattern of the 3D flow.

RECOMMENDATION

The results obtained can potentially be used in design and optimisation of horizontal and vertical axis wind turbine in which win turbine blades experience a wide range of AOAs.

ACKNOWLEDGEMENTS

This research was financially supported by the Ministry of Education and Science of Russian Federation (agreement No. 14.574.21.0151, unique identifier of applied scientific research RFMEFI57816X0151).

REFERENCES

Claessens, M.C., 2006. NACA 0018 measurement report. Master Thesis, Delft University of Technology, Delft, Netherlands.

Critzos, C.C., H.H. Heyson and R.W. Boswinkle Jr, 1955. Aerodynamic characteristics of NACA 0012 airfoil section at angles of attack from 0 deg to 180 deg (No. NACA-TN-3361). NASA, Washington, DC., USA. http://www.dtic.mil/docs/citations/ADA377080

Cummings, R.M., J.R. Forsythe, S.A. Morton and K.D. Squires, 2003. Computational challenges in high angle of attack flow prediction. Prog. Aerosp. Sci., 39: 369-384.

Dominy, R., P. Lunt, A. Bickerdyke and J. Dominy, 2007. Self-starting capability of a Darrieus turbine. Proc. Inst. Mech. Eng., Part A. J. Power Energy, 221: 111-120.

Eleni, D.C., T.I. Athanasios and M.P. Dionissios, 2012. Evaluation of the turbulence models for the simulation of the flow over a National Advisory Committee for Aeronautics (NACA) 0012 airfoil. J. Mech. Eng. Res., 4: 100-111.

Ferreira, C.J.S., A. Van Zuijlen, H. Bijl, G. Van Bussel and G. Van Kuik, 2010. Simulating dynamic stall in a Two-dimensional vertical-axis wind turbine: Verification and validation with particle image velocimetry data. Intl. J. Prog. Appl. Wind Power Convers. Technol., 13: 1-17.

Ferreira, C.S., G. Van Kuik, G. Van Bussel and F. Scarano, 2009. Visualization by PIV of dynamic stall on a vertical axis wind turbine. Exp. Fluids, 46: 97-108.

Gao, H., H. Hu and Z.J. Wang, 2008. Computational study of unsteady flows around dragonfly and smooth airfoils at low Reynolds numbers. Proceedings of the AIAA 46th International Conference on Aerospace Sciences Meeting and Exhibit, January 7-10, 2008, AIAA, Reno, Nevada, pp: 1-1.

Gregory, N. and C.L. O'reilly, 1973. Low-Speed Aerodynamic Characteristics of NACA 0012 Aerofoil Section, Including the Effects of Upper-Surface Roughness Simulating Hoar Frost. Her Majesty's Stationery Office, Richmond, London, UK., ISBN:9780114705268,.

Harris, C.D., 1981. Two-Dimensional Aerodynamic Characteristics of the NACA 0012 Airfoil in the Langley 8-Foot Transonic Pressure Tunnel. NASA Langley Research Center, Hampton, Virginia, Pages: 137.

Hoarau, Y., M. Braza, Y. Ventikos and D. Faghani, 2006. First stages of the transition to turbulence and control in the incompressible detached flow around a NACA0012 wing. Intl. J. Heat Fluid Flow, 27: 878-886.

Im, H. and G. Zha, 2011. Delayed detached eddy simulation of a stall flow over NACA0012 airfoil using high order schemes. Proceedings of the 49th International Conference on AIAA Aerospace Sciences Meeting Including the new Horizons Forum and Aerospace Exposition, January 4-7, 2011, AIAA, Orlando, Florida, pp: 1-1.

Jeong, J. and F. Hussain, 1995. On the identification of a vortex. J. Fluid Mech., 285: 69-94.

Jones, L.E., R.D. Sandberg and N.D. Sandham, 2008. Direct numerical simulations of forced and unforced separation bubbles on an airfoil at incidence. J. Fluid Mech., 602: 175-207.

Kirke, B. and L. Lazauskas, 2008. Variable pitch Darrieus water turbines. J. Fluid Sci. Technol., 3: 430-438.

Li, C., S. Zhu, Y.L. Xu and Y. Xiao, 2013. 2.5 D large eddy simulation of vertical axis wind turbine in consideration of high angle of attack flow. Renewable Energy, 51: 317-330.

Mary, I. and P. Sagaut, 2002. Large eddy simulation of flow around an airfoil near stall. AIAA J., 40: 1139-1145.

Moreau, S., J. Christophe and M. Roger, 2008. LES of the trailing-edge flow and noise of a NACA0012 airfoil near stall. Proc. Summer Program, 1: 317-329.

Sagaut, P., 2006. Large Eddy Simulation for Incompressible Flows: An Introduction. 2nd Edn., Springer, Berlin, Germany, Pages: 565.

Sheldahl, R.E. and P.C. Klimas, 1981. Aerodynamic Characteristics of Seven Airfoil Sections Through 180 Degrees Angle of Attack for Use in Aerodynamic Analysis of Vertical Axis Wind Turbines. Sandia National laboratories, Albuquerque, New Mexico.

Sheldahl, R.E., P.C. Klimas and L.V. Feltz, 1980. Aerodynamic performance of a 5-metre-diameter Darrieus turbine with extruded aluminum NACA-0015 blades. Master Thesis, National Technical Information Service, Springfield, Virginia, USA.

Sorensen, N.N. and J.A. Michelsen, 2004. Drag prediction for blades at high angle of attack using CFD. J. Solar Energy Eng., 126: 1011-1016.

Worasinchai, S., G. Ingram and R. Dominy, 2011. A low-Reynolds-number, high-angle-of-attack investigation of wind turbine aerofoils. Proc. Inst. Mech. Eng. Part. A. J. Power Energy, 225: 748-763.